

# Nanorods of silicon carbide from silicon carbide powder by high temperature heat treatment

B. B. Nayak · D. Behera · B. K. Mishra

Received: 29 August 2010/Accepted: 9 December 2010/Published online: 23 December 2010  
© Springer Science+Business Media, LLC 2010

**Abstract** Nanorods of silicon carbide were found to be produced directly from silicon carbide powder when subjected to high temperature heat treatment. The powder with 20–50 μm grain size was kept in a graphite crucible (enclosed in a chamber/furnace) and heated from its bottom at 2700 °C for 15 min by employing a typical configuration of arc plasma (Ar). The heating was then followed by chamber cooling (up to room temperature) for 2 h. Silicon carbide nanorods of 10–120 nm diameter and 5–20 μm length grew within the powder when the graphite crucible was kept 90% closed at its top end during the heat treatment. The heat treated powder and nanorods were evaluated by XRD, SEM, AFM, HRTEM and micro Raman spectroscopy. A catalyst (Fe) driven two stage VLS mechanism is proposed to understand the growth of the nanorods.

## Introduction

Silicon carbide (SiC) is a well known compound which has been researched over the last three to four decades towards replacing Si in high temperature semiconductor devices. The carbide shows very high hardness, high chemical resistance, excellent refractory and ceramic properties. The discovery of blue-light emission in SiC nano particle by quantum confinement [1, 2] drew serious attention of researchers in recent years with renewed interest. Experimental study has revealed [3] that SiC nanorods possess extremely high fracture strength that approaches the

theoretical limit and is much higher than the best values obtained in μm-diameter SiC whiskers. This property alone holds great promise for making ultra high strength nanocomposites of new kind [4] in polymer, metal and ceramic matrices [5]. The non-melting property of SiC associated with high dissociation temperature (~2200 °C) makes it suitable for semiconductor applications in high temperatures and at high power operations [4, 6]. SiC nanorods exhibit better field emission property and thus, emerge as a promising candidate for the development of field emission devices [7]. At present, use of SiC nanorods is limited to R&D for application in cold cathode field emission display (FED), such as field emission televisions, nanoelectronic devices and sensors [7, 8], but they have a promise in industrial usage (in nanocomposites) in near future. Dai et al. [9] have suggested that these nanorods are the ideal structures which could be used to pin vortices in high temperature superconductor.

SiC nanorods are prepared mostly by the following methods: carbon nanotube-based confining growth and high temperature reaction of carbon nanotube with SiH<sub>4</sub> or silicon compounds [8], chemical vapour deposition (CVD) [4, 8], chemical vapour growth (CVG) on SiC template [7], hydrothermal method [8], rf sputtering [7], carbothermal synthesis by reacting wood pulp template and carbon precursor [10], arc discharge [2], direct chemical reaction at low temperature and high pressure [4], carbothermal reduction of silica xerogels and halides [11] and pyrolysis of polycarbosilane on the surface of activated carbon [12]. SiC nanorods have also been prepared by hot filament CVD method and carbothermal reaction of SiO and Si at temperature above 1200 °C [8]. The template method [7] and the vapour-liquid-solid (VLS) catalyst synthesis method [8] are frequently used for growing various SiC nanostructures. This study reports a simple and inexpensive

B. B. Nayak (✉) · D. Behera · B. K. Mishra  
Institute of Minerals and Materials Technology, Council of  
Scientific & Industrial Research, Bhubaneswar 751013, India  
e-mail: bbnayak@immt.res.in; bijan\_nayak@yahoo.com

heat treatment method to produce SiC nanorods from SiC powder/grains. The process does not involve any high technology and is amenable for scaling up. Results of the nanorods growth and various characterisation studies are described and discussed in the article.

## Experimental

SiC does not melt but starts dissociating at around 2200 °C. The dissociation completes at 2825 °C. In this backdrop, it is aimed to heat treat SiC at the appropriate temperature for dissociation of Si from C, and then allow Si vapour to recombine with C (which does not melt at atmospheric pressure and above; M.P. of C is around 3800 °C in sub-atmospheric pressure) to produce SiC nanostructures. A typical configuration shown in Fig. 1 makes it an arc plasma to heat from the bottom of the graphite crucible. By using Ar as plasma forming gas, the arc can generate temperature up to 3000 °C in laboratory condition. The arrangement becomes a transferred arc plasma where the crucible works as the cathode and the plasma flame heats up the graphite crucible base from outside without causing interference in the charge (i.e. SiC powder) kept inside the crucible. Transformation of electrical energy to heat energy can take place up to 90% in this type of arc arrangement. SiC powder (Aldrich make, #409-21-2) of mixed phases ( $\alpha$  and  $\beta$ ) in 100 g scale (20–50  $\mu\text{m}$  grain size) were placed in the crucible before starting the heat treatment. The crucible was then closed (up to 90%) at the top end by a graphite lid (plate). The whole system was kept inside a chamber/furnace with provision for gas exhaust. The crucible base was heated to 2700 °C, which is above the boiling point of Si (2680 °C), by maintaining the arc conditions in the following range: voltage 40–50 V, current 500–550 A. Temperature of the graphite crucible was monitored by a two colour pyrometer (Mikron, model: M90-R3, accuracy:  $\pm 0.50\%$  of reading) focused through a port in the furnace wall. The heat treatment of SiC was carried out for 15 min, after which power was switched off in the arc to extinguish the plasma. Ar backup was provided for additional 30 min inside the chamber/furnace to prevent oxidation of the SiC grains. The chamber was allowed to cool for 2 h to attain room temperature.

Microstructural characterisations of the heat treated SiC powder were done by XRD (X-ray diffraction, diffractometer model: X'Pert Pro, Panalytical, Philips, Netherland), SEM (scanning electron microscope, attached with EPMA system: Jeol JXA-8100, Japan), AFM (atomic force microscope, attached with UMIS nanoindentation system, Fisher Cripps, Australia), TEM (transmission electron microscope, model: Tecnai G<sup>2</sup>, FEI, Netherland) and micro Raman spectrometer (model: inVia Reflex, Renishaw, UK,

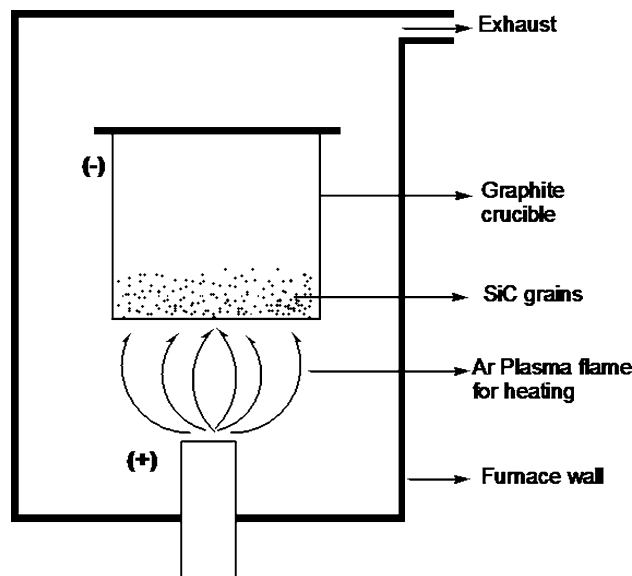


**Fig. 1** Schematic picture of arc plasma configured arrangement for heat treatment of SiC powder

Ar ion laser, 514 nm). For TEM study, ultrafine powder was first ultrasonically dispersed in methanol medium, and then it was transferred onto carbon coated copper grid for examination. AFM and micro Raman studies were carried out by employing circular araldite (polymer) mounts dispersed with SiC powder on their surfaces.

## Results

By heat treating the SiC powder at 2700 °C, nanorods of 10–120 nm diameter and 5–20  $\mu\text{m}$  length were produced. The nanorods were found to grow in clusters consisting of whisker-like agglomerate structures (Fig. 2) as well as

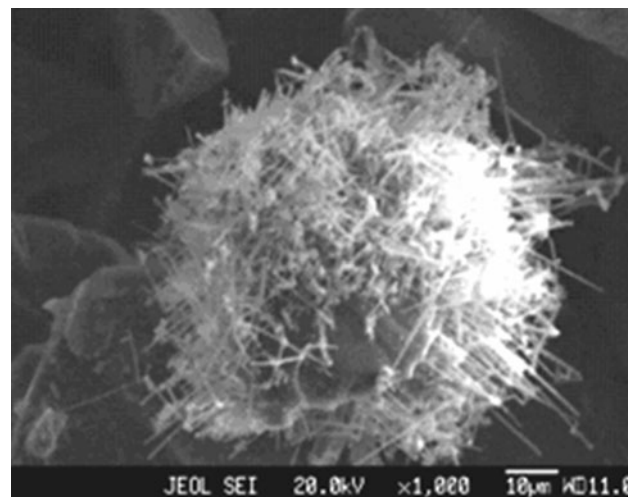


**Fig. 2** SEM image of SiC nanorods pinned on SiC grains

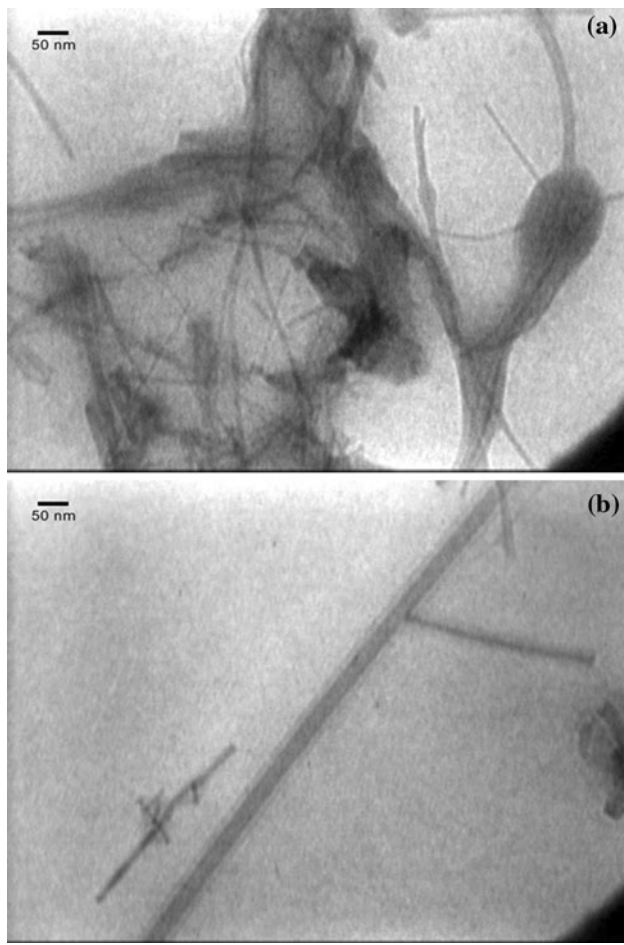


**Fig. 3** TEM pictures of SiC nanorods: **a** as grown rods in the sample, **b** an isolated rod with a right angled branch

unagglomerated nanorod forms (Figs. 3, 4). From the SEM picture of the typical SiC nanorod cluster (grown after heat treatment) shown in Fig. 2, it is seen that the rods are pinned on the grain surfaces. Besides the clustered growths,

unagglomerated nanorod growths are found at several other places. Figure 3a shows the TEM picture of unagglomerated nanorods with diameter in the range 10–30 nm which were grown after heat treatment. TEM picture of such a typical nanorod (~30 nm diameter) with a right angled branch (~20 nm diameter) is shown in Fig. 3b. The unagglomerated nanorods were also examined under AFM and some typical structures are shown in Fig. 4a, b. It is seen from the magnified view in Fig. 4b that the selected nanorod of around 115 nm diameter appears almost defect free; such kind of rod is desirable in electronic device applications. Figure 5a shows two nanorods (~30 and 50 nm, respectively in diameter) of similar morphology lying in two different planes. Few bridged/joined nanorods are observed under TEM in the heat treated samples, as shown in Fig. 5b, c. In Fig. 5b, the main rod and the right angled side growth (small one) are found almost same in diameter (~60 nm). A good nanorod (~50 nm diameter) appearing to be without any defect is seen in the TEM micrograph illustrated in Fig. 5d. Such rod has been chosen here for more investigation by selected area diffraction (SAD). X-ray diffraction patterns of the untreated and heat treated SiC powder/grains are shown and compared in Fig. 6. Major peaks due to  $\alpha$  and  $\beta$  phases of SiC as well as few small peaks due to graphite are observed. After heat treatment, the peak intensities are found to increase significantly in most of the cases. SAD taken on the upper tip region (rounded) of the rod (side growth) shown in Fig. 5b shows a  $d$  value of 0.250 nm which matches with SiC ( $\alpha/\beta$ ). The apparently defect free rod shown in Fig. 5d was observed under high resolution transmission electron microscope (HRTEM) at three different places: (i) at the upper tip of rod (fringe shown in Fig. 7a, observed in longitudinal position), (ii) at a place below the upper tip of rod but above the middle of rod stem (fringe shown in Fig. 8a, observed in lateral position) and (iii) at the middle

**Fig. 4** AFM images of SiC unagglomerated nanorods: **a** grown at several places in the sample, **b** an enlarged view of a typical nanorod showing defect free structure

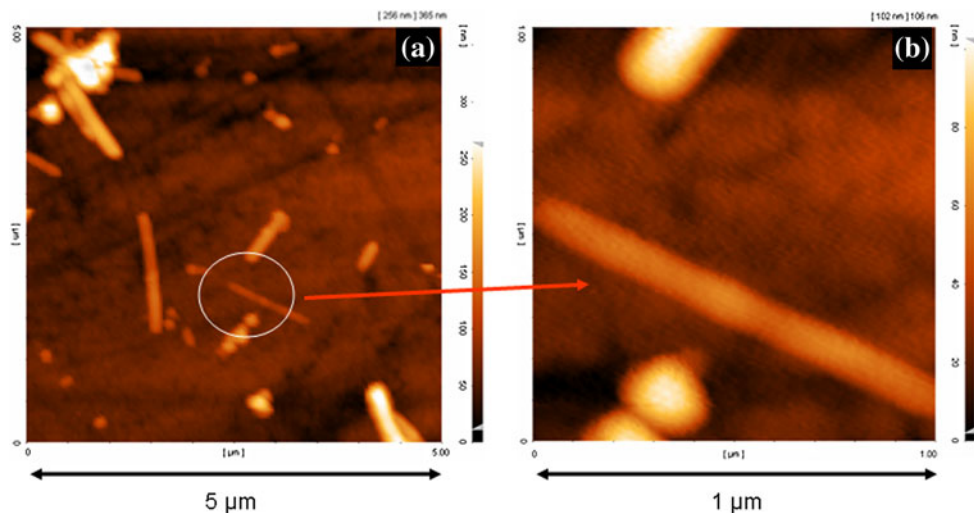


**Fig. 5** TEM pictures of different types of SiC nanorods grown (**a–d**) with SAD pattern shown in (**b**)

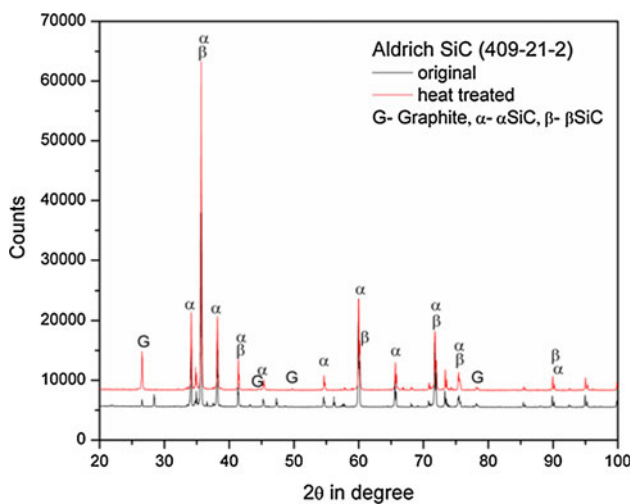
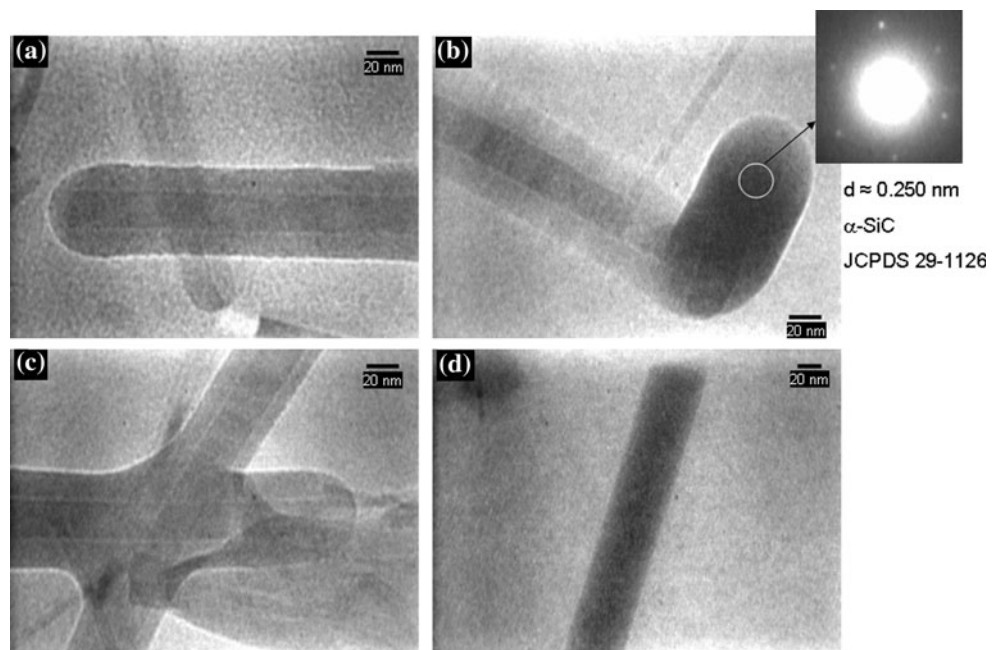


**Fig. 6** XRD of original powder (starting SiC) and the heat treated (at 2700 °C) SiC powder

of rod stem (fringe shown in Fig. 9, observed in longitudinal position) and SAD patterns were also recorded at these places. From the lattice fringes in Figs. 7a, 8a and 9, it is evident that the central core of the nanorod constitutes a crystalline structure comprising about 10 nm diameter zone around the longitudinal axis. From the SAD patterns shown in Figs. 7b and 8b, it is identified that the core consists of SiC. The SAD pattern shown in Fig. 8c was recorded outside but adjacent to the lattice fringe area (upper right hand corner of Fig. 8a) and it shows halo indicating the amorphous nature of grains. From lattice fringe in Fig. 7a, it is evident that lattice planes are arranged at an angle inclined to the transverse plane to the

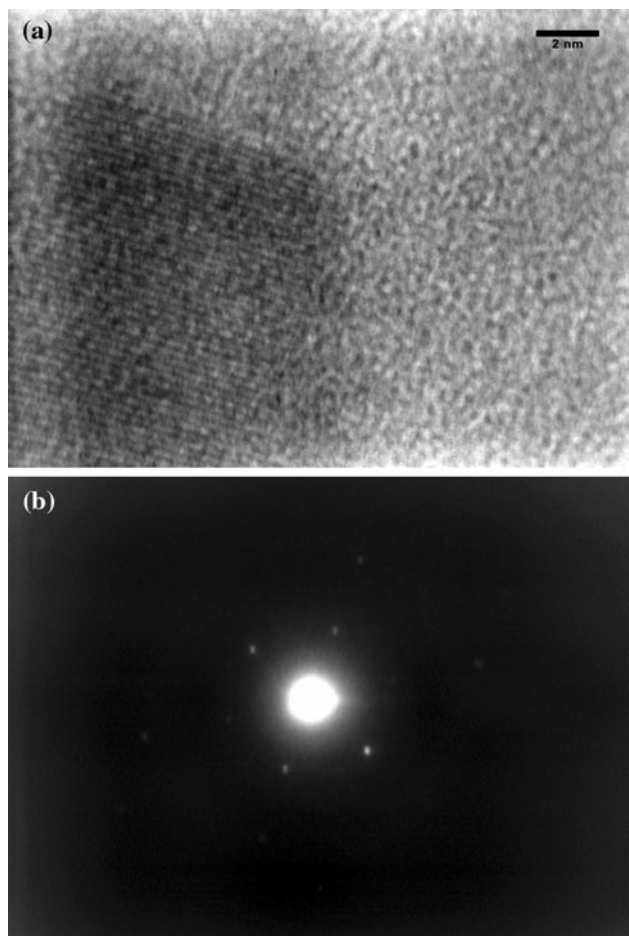


**Fig. 7** **a** HRTEM picture recorded at the upper tip of SiC nanorod (*longitudinal position*) shown in Fig. 5d. **b** SAD pattern recorded at the place described in (a) in the core zone of rod (*vertical position*)

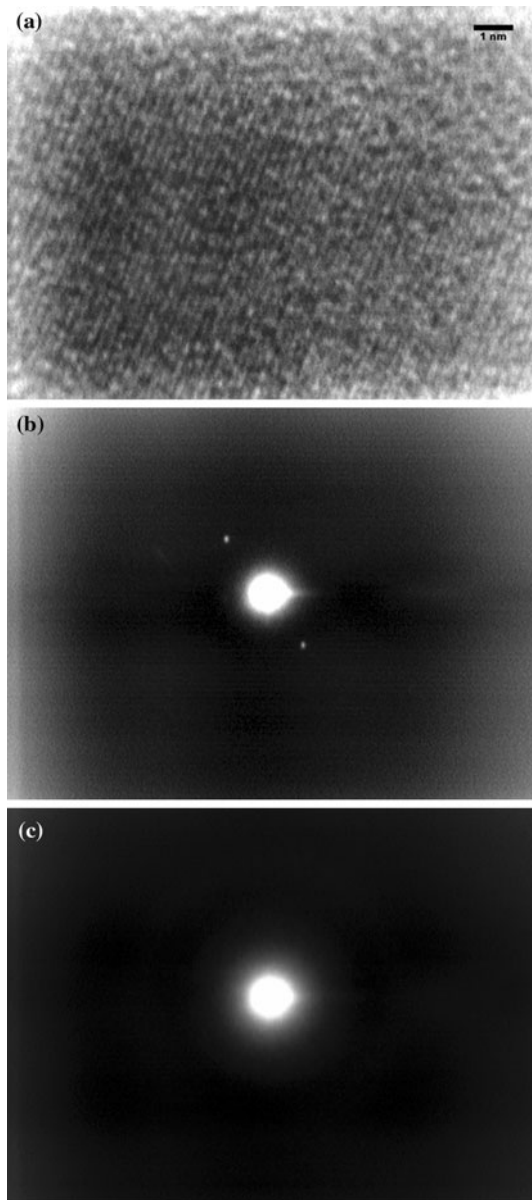


**Fig. 8** **a** HRTEM picture of SiC nanorod (*lateral position*), as shown in Fig. 5d, recorded at a place below the upper tip of rod but above the middle of rod stem. **b** SAD pattern recorded at the place described in (a) in the core zone of rod (*lateral position*). **c** SAD pattern recorded at a place outside but adjacent to the core zone (i.e. the co-axial sheath zone) of rod (*lateral position*) described in (a)

longitudinal axis of the nanorod. From the SAD pattern (Fig. 7b), it is found that the core of the rod exhibits reflection due to  $\alpha$  SiC ( $d = 0.2406$  nm) only. Figure 8a (observed in lateral position, located in the region of rod below the upper tip region but above the middle of rod stem) shows lattice fringes to occur along the transverse direction to the rod axis with an angle of inclination. This is similar to the first kind of finding as mentioned above (Fig. 7a). Figure 8b shows the corresponding SAD pattern of the core of the rod in this region. It shows reflection due

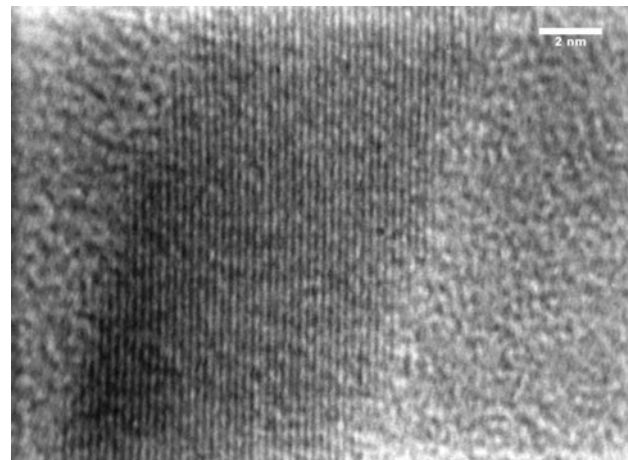


**Fig. 9** HRTEM picture of the SiC nanorod (as shown in Fig. 5d) recorded at the middle of its stem (*longitudinal position*)

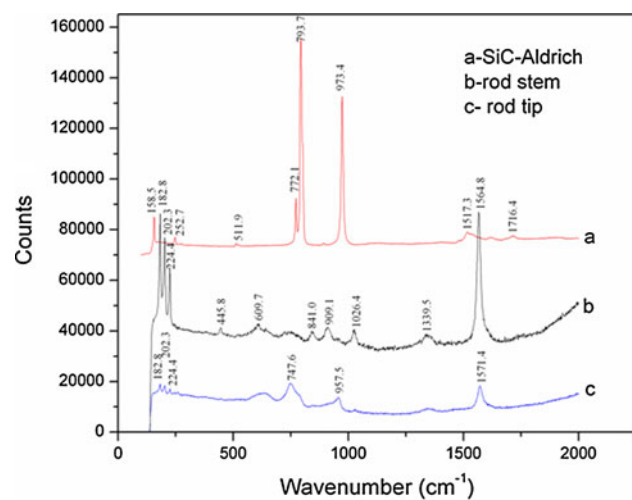


**Fig. 10** Micro Raman spectra of starting SiC powder/grain, SiC nanorod stem and tip

to  $\alpha$  SiC ( $d = 0.2393$  nm). Lattice fringes in Fig. 9 (recorded at the middle of rod stem, observed in longitudinal position) show that lattice planes in the central core of the rod are arranged at an angle inclined to the longitudinal axis which is unlike the earlier two cases. Micro Raman spectra of the SiC nanorods and grains were recorded using Ar ion laser and are shown in Fig. 10. Major peaks in the nanorod are observed at 609.7, 841, 909.1, 1026.4, 1339.5 and 1564.8 cm<sup>-1</sup> recorded at the middle of the rod stem where as 747.6, 957.5 and 1571.4 cm<sup>-1</sup> are the main peaks observed at upper end tip of the rod. SiC grains show main peaks at 973.4, 793.7 and 772.1 cm<sup>-1</sup>. Significant difference is marked between the spectra of the starting SiC grain and the nanorod; also, the intensities of the Raman peaks are found to be weak in case of nanorod compared to SiC grain. Intensity is observed

more reduced at the tip of the nanorod compared to the middle of the stem.

## Discussion

The high temperature heat treatment of SiC powder reported here is a new method for producing nanorods of SiC. Production of a temperature as high as 2700 °C ( $\pm 13.5$  °C) by employing an innovative arc plasma configuration, as shown in Fig. 1, is likely to reduce cost of processing and in some cases processing time compared to existing methods (e.g. rf sputtering, CVD, CVG, etc.). The method has a scope for easy scale up, hence could be employed for producing SiC nanorods in more quantity. The size (10–120 nm diameter) and length (5–20  $\mu\text{m}$ ) of the nanorods are suitable for application in nanocomposites for achieving high strength. The largely defect free nature (as seen in Figs. 4b, 5d) of the nanorod produced in this method prompts one to go for applications like nanoelectronic device (nanosensor), AFM tip and structure for pinning vertices in high temperature superconductors.

The nanorods produced after heat treatment are observed to grow in agglomerated (cluster type) and unagglomerated forms. The agglomerated lot appears like whisker kind growth but with nanorods pinned on grain surfaces (Fig. 2). On the other hand, the unagglomerated rods, which occur more in quantity, are found to be spread all over (Figs. 3a, 4a). Among these rods, few bridged/joined rods are seen in Fig. 5b, c which are similar to the structure observed by Pei et al. [8]. Right angled branch growths are also seen (Figs. 3b, 5b) in some rods. Mishra et al. [23] have explained that during growth of nanorods, small nanorods used to grow initially which then keep joining with each other to increase length. The joints emerge at the junction of two nanorods during such phenomenon. Minute observation of Fig. 5a, b and c shows that the nanorods in these figures are coaxial consisting of dense/dark core or central axial region (20–30 nm diameter) surrounded by less dense or grey zone (sheath). The core region consists of lamellar bands perpendicular to rod axis (may be attributed to stacking faults [12, 24–26]), thus ruling out the possibility of hollow structure like that exists in any nanotube. The cladded or core-sheath nanostructure has a scope to find application in optoelectronics [27] such as nanowire lasers (in UV region, due to wide band gap of SiC). From the XRD patterns of the untreated and heat treated SiC powder (Fig. 6), it is seen that the untreated SiC powder consists of mixed phases of SiC ( $\alpha$  and  $\beta$ ) along with small amounts of C in graphite phase. The heat treated powder shows significantly increased intensity in case of seven peaks including that of graphite. The increase in intensity may be attributed to reduction of defects upon

heat treatment. The  $d$  values obtained from XRD were found to be more appropriate to be identified with  $\alpha$  SiC (6H) [JCPDS: 29–1128, 1999]/ $\beta$  SiC (3C) [JCPDS: 29–1129, 1999]. While good number of peaks found in XRD makes it easy to identify various phases, the SAD patterns shown in Figs. 5b, 7b and 8b, c are characterised mostly by halos and few diffraction spots which make difficult to identify SiC phases. The authors have identified the spots as follows: the diffraction spots in Fig. 5b (due to the rounded tip small rod which is at right angle to the main rod) form part of a ring/circle corresponding to  $d = 0.250$  nm which may be assigned to  $\alpha$  SiC (6H), plane (102) [JCPDS: 29–1128, 1999]/ $\beta$  SiC (3C), plane (111) [JCPDS: 29–1129, 1999]/ $\alpha$  SiC (4H), plane (004) [JCPDS: 29–1127, 1999]/ $\alpha$  SiC (2H), plane (002) [JCPDS: 29–1126, 1999]. Similarly, from the diffraction spots around the halo in Fig. 7b (recorded at the upper end tip region of the defect free rod shown in Fig. 5d in longitudinal position), the ring corresponding to  $d = 0.2406$  nm is identified which may be attributed to  $\alpha$  SiC (6H), plane (103) [JCPDS: 29–1128, 1999]/ $\alpha$  SiC (4H), plane (102) [JCPDS: 29–1127, 1999]/ $\alpha$  SiC (2H), plane (101) [JCPDS: 29–1126, 1999]. Presence of  $\beta$  SiC (3C) [JCPDS: 29–1129, 1999] is ruled out here. Like wise, the diffraction spots in Fig. 8b (recorded in lateral position of the rod between the upper end tip and middle of rod stem) correspond to  $d = 0.2393$  nm which may be assigned to  $\alpha$  SiC only. The SAD pattern shown in Fig. 8c was recorded outside but adjacent to the lattice fringe area (upper right hand corner of Fig. 8a) and it shows halo without any diffraction spot. This indicates the amorphous nature of the grains outside the central/axial core region of the nanorod. In view of the more proximity of the  $d$  value of 0.250 nm (in SAD shown in Fig. 5b) to  $\alpha$  SiC (6H/4H/2H) than to  $\beta$  SiC (3C), and also due to identification of only  $\alpha$  SiC phase in the SAD patterns of Figs. 7b and 8b, the occurrence of  $\beta$  SiC (3C) (as seen in the SAD shown in Fig. 5b) in the nanorod may be remote. Taking into account the results of the lattice fringe and SAD patterns discussed above, it is evident that the core or central axial region of the nanorod (shown in Fig. 5d) constitutes crystalline  $\alpha$  SiC being spread over a zone of around 10 nm in diameter. It is then surrounded by an amorphous sheath (cladding) or co-axial zone of around 20 nm thickness. Since micro Raman spectra of the nano rod stem (in the middle part) observed at 609.7, 841, 909.1, 1026.4, 1339.5 and 1564.8  $\text{cm}^{-1}$  and of the nanorod tip observed at 747.6, 957.5 and 1571.4  $\text{cm}^{-1}$  (Fig. 10) do not match with silica lines (503, 467 and 215  $\text{cm}^{-1}$ ) or quartz lines (768, 790 and 968  $\text{cm}^{-1}$ ), the possibility of silicon oxide constituting the sheath does not hold good. Raman spectra of SiC nanorod has been discussed in literature by several workers [8, 12, 28] and the lines 784.7 and 796  $\text{cm}^{-1}$  (TO mode) and 915.1 and 972  $\text{cm}^{-1}$  (LO mode)

are identified with  $\beta$  SiC. Free carbon shows Raman peaks between 1300 and 1600  $\text{cm}^{-1}$  and graphite shows peaks at 1329.8 and 1568.8  $\text{cm}^{-1}$  [8]. Diamond shows peak at around 1332  $\text{cm}^{-1}$ , nanocrystalline diamond shows peak at 1130  $\text{cm}^{-1}$  and DLC (diamond-like carbon) broad band at 1485  $\text{cm}^{-1}$  [29]. However, the library (available with the inVia Reflex Raman spectrometer, Renishaw, UK) shows that the green silicon carbide ( $\alpha$  phase) exhibits Raman lines at 797, 1002 and 1527  $\text{cm}^{-1}$ . In view of above and also taking cognizance of the possibility of Raman shift due to residual stress and quantum size confinement in nanorod [8], unambiguous identification of the Raman spectra, shown in Fig. 10, seems difficult, however, in view of considerable reliability of molecular spectra in nano/micro domain compared to XRD and EDS (energy dispersive spectra of X-ray), one may conclude that the surface layer of the nanorod is an amorphous layer composed of SiC and dissociated C in the form of DLC and graphite. The amorphous layer (confirmed from SAD) surrounding the crystalline SiC core as a sheath extends over a thickness of around 20 nm. Amorphous structure growth may be attributed to faster cooling of the nanorod surface compared to its core. A comparison of spectra of rod stem (Fig. 10b) and rod tip (Fig. 10c) with grain (Fig. 10a) shows distinct differences, particularly in respect of appearance of new prominent peaks at 1564.8 and 1571.4  $\text{cm}^{-1}$  respectively. The variation in Raman spectra pattern between tip and stem could be due to occurrence of double curvature at the tip.

The lattice fringes observed in Figs. 7a, 8a and 9 show that lattice planes undergo change in orientation from tip end to middle of stem in the nanorod. At the tip region, the planes are found transverse to length axis with a small angle of inclination. However, at the middle of the stem, they are oriented longitudinally with small angle of inclination to the length axis. Gao et al. [26] have reported SiC nanorod growth with lattice planes oriented along [111] axis direction and also along axis normal to [111] direction. According to them, while the axial direction growth may be assisted by rough tip surface, the axis normal growth may be assisted by stacking fault. In this case, the near longitudinal/axial growth of lattice planes takes place in the middle of the nanorod stem which is quite away from the rough tip, thus the suggestion of Gao et al. may not be applicable.

Several works have been reported in literature on the growth of one dimensional nanostructures and addressed issues like effect of monomer concentration on the shape of semiconductor quantum dots (QDS), vapour-liquid-solid (VLS) growth for nanowires by CVD and PVD methods, light induced shape change mechanism of metal nanorods [13], etc. Wu et al. [5] have proposed a vapour solid (V-S) mechanism for  $\beta$  SiC nanorod growth where Si vapour

diffuses into carbon nanotube (CNT) and reacts with C to form nanorod in the direction of CNT. Recently, Cheong and Lockman [14] have suggested a six stage V-S mechanism to explain the growth of 3C-SiC ( $\beta$  SiC) nanowires from heated Si substrate and activated carbon under vacuum condition at 1200–1350 °C. Wagner and Ellis [15] were the first to suggest a VLS mechanism for the growth of SiC whiskers initiated by a metal catalyst. This was supported by later workers [16, 17] who produced  $\mu\text{m}$ -size SiC whiskers. Belmonte et al. [18], on the other hand, reported the growth of SiC whiskers from a Si-rich liquid. Seeger et al. [2], while growing nm-sized  $\beta$  SiC whiskers in direct arc discharge, suggested a two stage VLS growth mechanism initiated by Fe catalyst. In the light of the experimental finding, a growth mechanism for  $\alpha$  SiC nanorod is suggested here to understand the results.

After treatment in the arc plasma heated graphite crucible at 2700 °C, SiC dissociates and out of the two dissociated species in this compound, Si goes to vapour state because its boiling point is 2680 °C. However, C does not melt (M.P of C: ~3800 °C), nor it vaporizes (B.P of C: 4830 °C) at such heat treatment temperature of 2700 °C; hence it remains in the parent lattice. As seen from Fig. 1, the typical configuration involving a lid on the top of the crucible was marked to be crucial for nanorod growth. When the crucible was kept full open at its top end, no nanorod growth was observed from the SiC grains but when the lid was made closed on the crucible top up to 90%, nanorods were found to be produced. This suggests that Si vapour plays a key role in the growth process of the SiC nanorods. Usually SiC powder produced by various commercial companies contain small quantity of Fe as impurity [19–21] and therefore, the Aldrich SiC (grade 409-21-2) used in this study was analysed by X-ray fluorescence (XRF) method and was found to contain 0.1 wt% Fe. In the light of the above detection of Fe, a two stage VLS mechanism initiated by Fe catalyst is proposed. Although few works have been reported in literature [11, 30–32] regarding the catalytic role of elements like Ni, Co, transitional elements, La, etc. in the growth of SiC nano-whiskers and nano-fibres, no effort was done in this study to find the effect of those catalysts. When plasma heat treatment of SiC grains is done at 2700 °C, the impurity Fe contained in the SiC goes to liquid state since its melting point and boiling point are 1539 °C and 2861 °C, respectively. Once plasma heating is stopped, the SiC grains undergo simultaneous cooling along with reactor chamber/furnace (up to room temperature). Just after switching off the power in the arc, cooling proceeds from 2700 °C towards lower temperatures. Between 2700 °C and 2680 °C (B.P of Si), the Si exists in vapour form and reacts with solid C (dissociated from SiC) to form SiC. At this stage, in situ Fe exists in liquid state (small in quantity:

around 0.1 wt% Fe) and is available in the dissociated SiC grains both on grain surfaces and vicinity in small quantities to act as catalyst during nucleation and growth of nanorods or nanowiskers by reaction of Si vapour with the dissociated C available. Such mechanism is not far fetched because in this experiment it has been observed that SiC nanorods are found to be pinned on grain surfaces (Fig. 2) and also formed in the vicinity of grains (Figs. 3, 4, 5). It may be pointed out here that because the B. P. of Si stands at 2680 °C and complete dissociation of SiC takes place at 2825 °C, a heat treatment temperature more than 2700 °C (employed in this investigation) but not exceeding 2825 °C, is likely to improve the nanorod growth performance with rise of temperature. This will be due to enhanced degree of dissociation of SiC at higher temperature that would increase the partial pressure of Si vapour which results in the availability of more number of Si atoms to react with dissociated C atoms lying in the lattice. However, 2680 °C, the B. P. of Si, being lower than 2825 °C, the dissociation temperature of SiC, any heat treatment temperature beyond 2825 °C cannot improve the nanorod growth performance further if pressure in the reactor is not allowed to change from 1 bar. Chrysanthou et al. [22] have reported possibility of SiC whisker nucleation occurring on Fe catalyst. Seeger et al. [2] also described Fe catalyst use in arc discharge to grow nano SiC whiskers. In such a backdrop, it may be stated that SiC nanorod growth from SiC powder can take place by employing high temperature heat treatment in the range 2680–2825 °C using a crucible heating method by typical arc plasma configuration. Reaction of dissociated Si vapour with the dissociated C lying in SiC lattice in presence of in situ Fe (playing catalyst role) seems to be the mechanism responsible for the formation of SiC nanorod. The nanorod forms during chamber/furnace cooling between heat treatment temperature (need to be more than B. P. of Si) and 2680 °C, the B.P. of Si.

## Conclusion

SiC nanorods have been produced for the first time directly from SiC powder by heat treatment of mixed phase ( $\alpha$  and  $\beta$ ) SiC powder at 2700 °C by employing an arc plasma (Ar) configured heating in a graphite crucible followed by chamber cooling up to room temperature. Nanorods of 10–120 nm diameter and 5–20  $\mu\text{m}$  length grow by this process. HRTEM analysis of a typical 50-nm-diameter nanorod shows the microstructure to consist of a coaxial structure composed of nanocrystalline  $\alpha$  SiC lying in the central/axial zone of 10 nm diameter being surrounded by an amorphous sheath zone of 20 nm thickness. The nanorod formation/growth may be understood by a catalyst (Fe)

initiated two stage VLS mechanism. The process is simple, low cost and amenable for scale up.

## References

- Zhang Z (1998) *Micros Res Tech* 40:163
- Seeger T, Redlich PK, Ruhle M (2000) *Adv Mater* 12:279
- Wong EW, Sheehan PE, Lieber CM (1997) *Science (Washington DC)* 277:1971
- Yang W, Miao H, Xie Z, Zhang L, An L (2004) *Chem Phys Lett* 383:441
- Wu RB, Yang GY, Pan Y, Chen JJ (2007) *J Mater Sci* 42:3800. doi:[10.1007/s10853-006-0461-5](https://doi.org/10.1007/s10853-006-0461-5)
- Brosselard P, Banu V, Camara N, Perez-Thomas A (2009) *Mater Sci Eng B* 165:15
- Xu D, He Z, Guo Y, Wang Y (2006) *Microelectron Eng* 83:89
- Pei LZ, Tang YH, Zhao XQ, Chen YW (2007) *J Mater Sci* 42:5068. doi:[10.1007/s10853-006-0390-3](https://doi.org/10.1007/s10853-006-0390-3)
- Dai H, Wong EW, Lu YZ, Fan S, Lieber CM (1995) *Nature (London)* 375:769
- Shin Y, Wang C, Samuels WD, Exarhos GJ (2007) *Mater Lett* 61:2814
- Huczko A, Lange H, Bystrzejewski M, Rummeli MH, Gemming T, Cudzilo SC (2005) *Cryst Res Technol* 40:334
- Li G, Li X, Wang H, Xing X, Yang Y (2010) *Mater Sci Eng B* 166:108
- Burda C, Chen XB, Narayanan R, El-Sayed MA (2005) *Chem Rev* 105:1025
- Cheong KY, Lockman Z (2009) *J Nanomater*. 5 pp. doi:[10.1155/2009/572865](https://doi.org/10.1155/2009/572865)
- Wagner RS, Ellis WR (1965) *Trans Met Soc AIME* 233:1053
- Bootsma GA, Knippenberg WF, Verspui G (1971) *J Cryst Growth* 11:297
- Narisco-Romero FJ, Rodriguez-Reinoso F (1996) *J Mater Sci* 31:779. doi:[10.1007/BF00367899](https://doi.org/10.1007/BF00367899)
- Belmonte T, Bonnetaire L, Jinoux JL (1996) *J Mater Sci* 31:2367. doi:[10.1007/BF01152948](https://doi.org/10.1007/BF01152948)
- Nayak BB, Mohanty BC, Singh SK (1996) *J Am Ceram Soc* 79:1197
- Bresker RI, Voronin NI, Khrycheva DD (1963) *Refract Ind Ceram* 4:93
- Coppola JA, Lawler HA, McMurtry CH (1978) US Patent 4123286
- Chrysanthou A, Grieveson P, Jha A (1991) *J Mater Sci* 26:3463. doi:[10.1007/BF00557132](https://doi.org/10.1007/BF00557132)
- Mishra SB, Mishra AK, Crause RW, Mamba BB (2009) *J Am Ceram Soc* 92:3052
- Pan Z, Lai HL, Au FCK, Duan X, Zhou W, Shi W, Wang N, Lee CS, Wong NB, Lee ST, Xie S (2000) *Adv Mater* 12:1186
- Yang W, Araki H, Kohyama A, Thavee Thavorn S, Suzuki H, Noda T (2004) *J Am Ceram Soc* 87:1720
- Gao YH, Bando Y, Kurashima K, Shato T (2000) *J Electron Microsc* 49:641
- Law M, Goldberger J, Yang P (2004) *Annu Rev Mater Res* 34:83. doi:[10.1146/annurev.Matsci.34.040203.112300](https://doi.org/10.1146/annurev.Matsci.34.040203.112300)
- Feng X, Chen Z, Ma J, Zan X, Pu H, Lu G (2003) *Optic Mater* 23:39
- Nayak BB (2004) *Surf Eng* 20:139
- Chen YF, Liu XZ, Deng XW (2010) *J Mater Sci Technol* 26:1041
- Pickard SM, Derby B, Feest EA (1991) *J Mater Sci* 26:6207. doi:[10.1007/BF01113906](https://doi.org/10.1007/BF01113906)
- Hao YJ, Jin GQ, Han XD, Gyo XY (2006) *Mater Lett* 60:1334